Performance Comparison of Square and Split Heaters

Min Soo Kim, Bang Weon Lee, Yong Soo Lee, Dong Kee Sohn, Dong Sik Shim and Keon Kuk; Micro Device & Systems Lab., Samsung Advanced Institute of Technology (SAIT); Yongin, Gyeonggi 446-712, Korea

Abstract

We investigated performance of square and split heaters experimentally. Four micro heaters were prepared. They included two square heaters, S20 (20μm×20μm) and S24 (24μm×24μm), and two split heaters, D22 (22μm×10μm×2) and D26 (26μm×12μm×2). Square and split heaters showed similar characteristics in electrical strengths irrespective of size and electric resistance. Heater shape seemed to have little influence on the actuating performance. Temperature on the heater surface was measured using an infrared (IR) microscope. Larger thermal spreading was observed on the split heater. The split heater is expected to manage relatively higher energy compared to the square heater of similar size.

INTRODUCTION

Many studies have been done on micro heaters and bubbles on them. They contributed understanding of bubble generation mechanism and actuating characteristics. Asai [1] proposed the bubble nucleation theory to provide a guide to the design of thermal inkjet heads, and Andrews [2] showed the complete bubble cycles from nucleation to collapse by visualization techniques. Rembe *et al.* [3] visualized the non-reproducible phenomena in micro heater with real high speed cine photomicrography. Kuk *et al.* [4] studied the thermal efficiency of micro heaters, especially effects of heater size and aspect ratio. More recently, Kim *et al.* [5] compared the actuating characteristics of non-passivated and passivated heaters.

In the present study, performance of square and split heaters was investigated in terms of actuating efficiency and thermal spreading capability. Four kinds of micro heaters were prepared and toughness of the fabricated heaters was compared by step-stress test (SST). Open pool bubble visualization gave bubble volume. Numerical simulation based on the hybrid nucleation model [5] and the Asai's model [6] provided actuating efficiency. Finally, through micro infrared (IR) temperature measurement, thermal spreading capabilities were estimated and compared.

METHODS

Preparation of Micro Heaters

Micro heaters were fabricated using conventional photolithographic techniques (Figure 1). Thermal barrier layer of silicon dioxide (SiO_2) of 2μm was thermally grown on silicon wafer. Tantalum nitride (TaN) heater and aluminum (Al) electrode were consecutively deposited by sputtering. The sheet resistance of TaN film was about 65Ω/square. Silicon nitride (SiN_x) film of 3000Å was deposited using PECVD technique as a passivation layer. Finally, tantalum (Ta) film of 3000Å was deposited as an anti-cavitation layer. Four kinds of micro heaters were prepared (Table 1).

Step-stress test (SST) was carried out to obtain relation between power density and pulse width [4, 5]. Cutoff pulse width was estimated as maximal one before causing more than about 5% variation from the initial resistance.

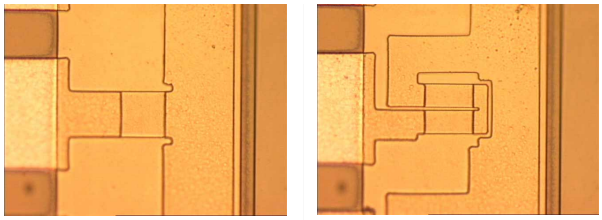

(a) (b)

Figure 1. Optical microscope images of the fabricated micro heaters; (a) Square heater; 24μm×24μm and (b) Split heater; 26μm×12μm×2ea. Both have SiO_2 of 2μm, SiN_x of 3000Å and Ta of 3000Å.

Table 1. Four different micro heaters.

Type	ID	Size W×H (μm)	Area (μm^2)	Resistance (Ω)
Square	S20	20×20	400	65
	S24	24×24	576	65
Split	D22	22×10×2	440	265
	D26	26×12×2	624	265

Open Pool Bubble Visualization

Bubbles on the heaters were visualized in an open pool setup shown in Figure 2. Bubble was synchronized with input pulse to the heater, and bubble images were captured by high speed CCD cameras [7]. Estimation of the bubble volume requires two synchronized bubble images; plane and side views with two CCD arrangements as shown in Figure 3 [4, 5].

Electrical heating pulses of square wave were applied to the micro heaters with 8 Hz repetition frequency. Electrical power multiplied by the pulse width represents input energy to the heater [8]. Bubble volume was obtained as a function of time through elaborating image processing with both plane and side views of bubble taken experimentally [4, 5]. Work by bubble formation was estimated following the same procedure in our previous article [4, 5]. Finally, actuating efficiency could be obtained as bubble work divided by input energy.

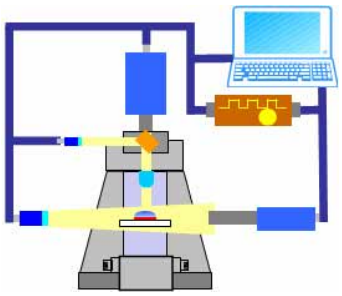

Figure 2. Experimental setup for open pool bubble visualization.

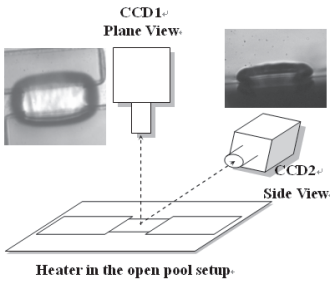

Figure 3. Two CCDs for capturing both plane and side views of bubble.

Micro Infrared (IR) Temperature Measurement

Infrared microscope (InfraScope II, QFI Co.) was used for temperature measurement. Image sensor made of indium antimonite (InSb) had a working wave length from 2 to 5µm, optimized for high optical resolution at low temperature. The image sensor had 512×512 pixels and resolution of 1.08 µm/pixel for the magnification used in this study. Base temperature was controlled up to 70°C by a heated stage to minimize environmental thermal noise.

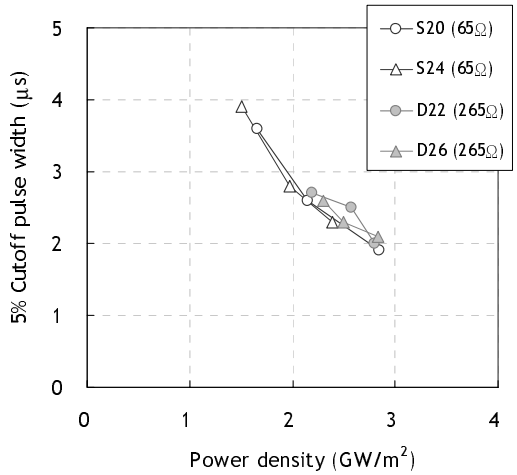

Figure 4. SST results of four micro heaters showing 5% cutoff pulse width as a function of driving power density.

RESULTS AND DISCUSSIONS

Relation between Power Density and Pulse Width

Figure 4 depicts cutoff pulse width as a function of power density. All the results from four different heaters were on the same line. Cutoff pulse width decreased with increasing power density. Both heater size and shape had little effects on cutoff pulse width. Besides, electric resistance seemed to have little influence on SST results.

Bubble Work and Actuating Efficiency

Estimated bubble work and actuating efficiency are presented in Figure 5. Each driving condition for different heaters corresponds to similar power density of 2.4 to 2.7GW/m^2. Split heater was 8 to 10% larger in size than the corresponding square heater (Table 1). However, they produced similar work (Figure 5a). Bubble work increased with increasing energy density, showing more increase for larger heater.

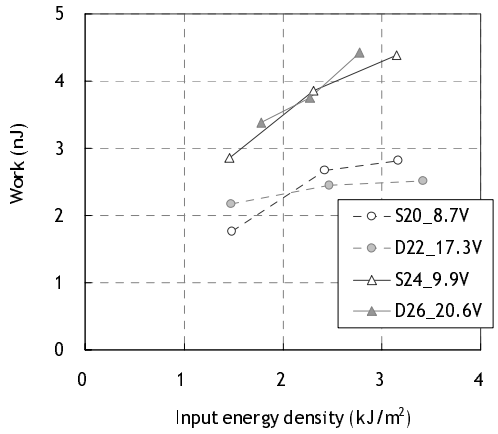

(a)

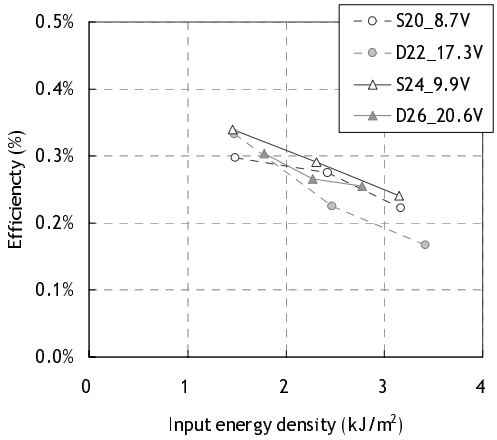

(b)

Figure 5. (a) Work done by bubble actuation and (b) actuating efficiency defined as bubble work relative to input energy.

At the same energy density, more bubble work was produced from larger heater. However, actuating efficiencies were similar with each other (Figure 5b). This implies that the amount of increase in total energy corresponding to the increased bubble work was accompanied with larger heater. On the other hand, actuating efficiency decreased with increasing energy density.

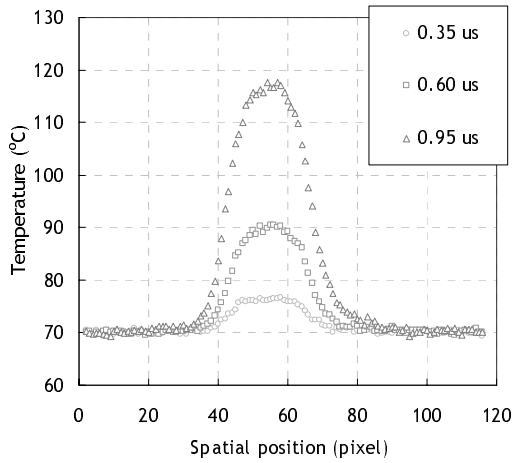

(a)

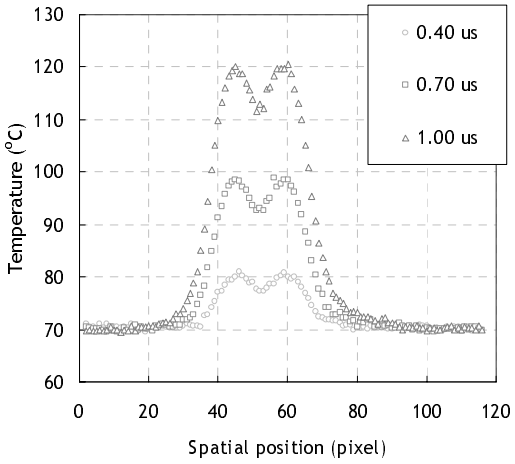

(b)

Figure 6. Typical spatial temperature profiles from micro IR temperature measurement; (a) Square heater, S24 with 9.9V at 3kHz and (b) Split heater, D26 with 19.6V at 3kHz. Different values of pulse width were tested. One pixel corresponds 1.08μm.

Thermal Spreading Capability

Figure 6 shows typical temperature profiles around heaters obtained from micro IR temperature measurement. Equivalent temperature profile was obtained when the heater was driven with a prescribed electrical pulse at a frequency of 3 kHz. Base temperature was set to 70°C for all cases. Different values of pulse width were used, which were tested in the open pool bubble visualization.

Temperature profiles on square heater, S24 and split heater, D26 are depicted in Figures 6a and 6b, respectively. Symmetrical temperature distributions were clearly seen about the heater center. In the split heater, maximum temperatures were located on around center of each heater strip, not on the slit between them.

Ratio of planar thermal spreading area relative to heating area is presented as a function of energy density in Figure 7. Thermal spreading area is defined as thermally affected region above reference temperature. Reference temperature, T_{ref}, was chosen as 75°C. Here, heating area represents size of heater envelope including gap between two heater strips. For example, heating area is 484 (=22×22) μm^2 for D22.

Results clearly showed higher thermal spreading ratio in the split heaters. For either square or split heater, heater size seemed to have no influence on the thermal spreading ratio.

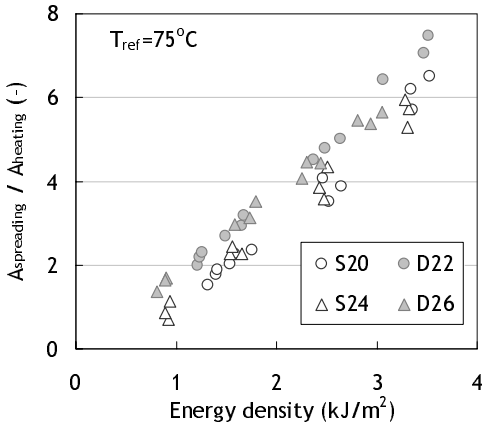

Figure 7. Ratio of effective thermal spreading area relative to heating area.

Figure 8 presents temperature profiles normalized by temperature difference, $(T-T_b)/(T_{max}-T_b)$ for cases of S20 and D22. Thus, normalized temperature has values between 0 and 1. Each graph contains data obtained from five different heaters and the corresponding Gaussian profile. From Figure 8, value of full width-half maximum (FWHM) could be estimated. Figure 9 depicts the FWHM of S20 and D22 normalized by the corresponding heater width for several different values of base temperatures, T_b. Higher thermal spreading capability of split heater was confirmed again, especially irrespective of base temperature.

This might be explained by the difference in shapes of temperature profiles. In split heaters, local maximums of equivalent temperature exist around center on each heater strip (Figure 6). Thus, temperature profile on the split heater becomes much closer to the shape of square wave (Figure 6b and Figure 8b). This means much steeper temperature gradient in the heater planar direction. Therefore, heat transfer to the surroundings can be enhanced to give larger thermal spreading in the split heater.

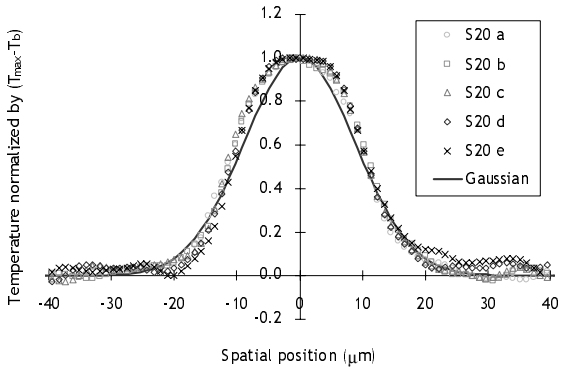

(a)

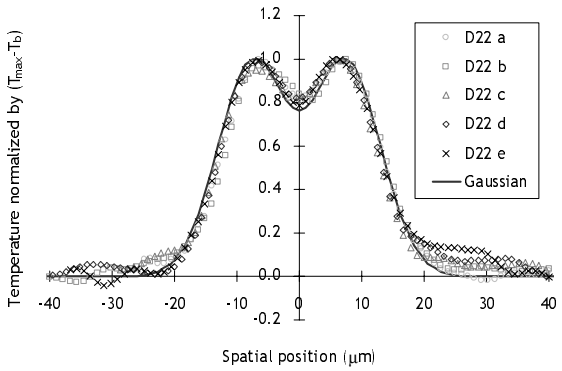

(b)

Figure 8. Temperature profiles normalized by (T_{max}–T_b); (a) Square heater, S20 with 8.7V, 0.7μs at 3kHz and (b) Split heater, D22 with 17.3V, 0.75μs at 3kHz. Each contains data from five heaters and the corresponding Gaussian profile.

CONCLUSIONS

Results from SST showed that toughness of micro heater is hardly affected by heater size and shape as well as electric resistance. Split heater could produce similar actuating force and efficiency with square heater. Careful comparison of temperature profiles using micro IR system revealed a little more thermal spreading in split heaters. Split heater might be favorable for higher energy (or frequency) operation because of better thermal spreading capability. Present study will help design of thermal inkjet heads of higher performance.

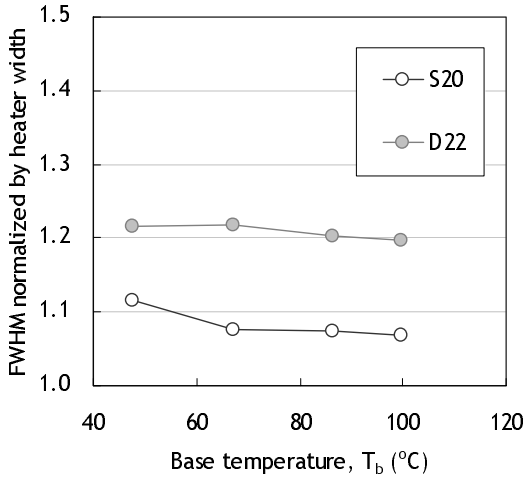

Figure 9. FWHM from Figure 8 normalized by heater width at several different values of base temperature, T_b.

References

1. A. Asai, Jpn. J. Appl. Phys., 28(5), 909-915 (1989).
2. J. R. Andrews, IMA Workshops, Minneapolis, MN (IMA, Cambridge, UK, 2001).
3. C. Rembe, S. Wiesche, M. Beuten, and E. P. Hofer, Proc. SPIE 3409, 316-325 (1998).
4. K. Kuk, J. H. Lim, M. S. Kim, M. C. Choi, C. H. Cho, and Y. S. Oh, "Research on Micro Heater Efficiency for Thermal Inkjet Head," J. of Imaging Science and Technology, 49(5), 545-549 (2005).
5. M. S. Kim, B. W. Lee, Y. S. Lee, D. S. Shim, and K. Kuk, "Effects of Thin Film Layers on Actuating Performance of Micro Heaters," NIP22; 22nd International Conference on Digital Printing Technologies, Denver, Colorado, USA, Sep. 17~22, pp. 61-65 (2006).
6. A. Asai, "Bubble Dynamics in Boiling under High Heat Flux Pulse Heating," J. of Heat Transfer, 113, 973-979 (1991).
7. C. Rembe, J. Patzer, E. Hofer, and P. Kreh, J. of Imaging Science and Technology, 40(5), 400-404 (1996).
8. J. H. Lim, Y. S. Lee, H. T. Lim, S. S. Baek, K. Kuk, and Y. S. Oh, Proc. IEEE MEMS Conference, 197-200 (IEEE, Piscataway, NJ, 2003).

Author Biography

M.S. Kim received his Ph.D. degree in Mechanical Engineering from Seoul National University (SNU), Seoul, Korea in 1998. After one and half year as a post-doctoral research fellow at Kyoto University (KU), Kyoto, Japan, he joined Samsung Electronics Co. Ltd. (SEC), Korea in 2000, and has been with Samsung Advanced Institute of Technology (SAIT), Korea since 2001. His scientific interests include micro thermo-fluidics, inkjet printing and MEMS.